

Article

Insights into Alpine-Karst-Type Tufa Deposits in Geological Environmental Records: A Case Study of the Calcareous Tufa Profile of the Jiuzhaigou Natural Reserve on the Eastern Margin of the Tibetan Plateau

Congcong Lv ¹, Xueqin Zhao ^{1,*}, Yaoxi Jiang ¹, Heyan Zhu ¹, Hongmin Zhang ², Fudong Wang ^{1,*}, Qiongfang Li ³ and Keli Hou ¹

¹ School of Environment and Resources, Southwest University of Science and Technology, Mianyang 621010, China

² Sichuan Railway Construction Co., Ltd., Chengdu 610072, China

³ School of Life Science and Engineering, Southwest University of Science and Technology, Mianyang 621010, China

* Correspondence: zhaoxq@swust.edu.cn (X.Z.); wolfdongswust@163.com (F.W.)

Abstract: To study the geological environmental records of alpine-karst-type tufa deposits in the eastern margin of the Tibetan Plateau, the calcareous tufa profile exposed by the “8.8” Jiuzhaigou earthquake was taken as the research object and combined with a field geological investigation. Further, the petrography, sedimentology, chronology, and elemental geochemistry of the calcareous tufa were studied and analyzed. The results show the following. (1) The Sparkling Lake calcareous tufa profile was deposited under the background of a warm and humid climate during the Holocene. The growth pattern follows a bottom-to-top deposition. (2) At 750 ± 30 – 300 ± 30 aB.P., the calcareous tufa layers were gray-black as a whole, and the changes in mineral composition and elemental geochemistry indicate a fluctuating upward trend for temperature and precipitation during this period. (3) The formation of two sets of black peat layers in the upper part of the tufa calcareous profile is due to the synergistic action of multiple factors caused by strong tectonic activity. In conclusion, the deposition mechanism of the calcareous tufa in Jiuzhaigou was controlled by paleoclimate hydrology and glaciation for a long time, while strong tectonic activity over a short period of time considerably changed the color, structure, element content, and mineral composition of the calcareous tufa.

Keywords: calcareous tufa; carbon-oxygen isotopes; tectonic activity; geological environment; Holocene



Citation: Lv, C.; Zhao, X.; Jiang, Y.; Zhu, H.; Zhang, H.; Wang, F.; Li, Q.; Hou, K. Insights into Alpine-Karst-Type Tufa Deposits in Geological Environmental Records: A Case Study of the Calcareous Tufa Profile of the Jiuzhaigou Natural Reserve on the Eastern Margin of the Tibetan Plateau. *Minerals* **2023**, *13*, 120. <https://doi.org/10.3390/min13010120>

Academic Editors: Francesca Giustini, Mauro Brilli and Santanu Banerjee

Received: 15 September 2022

Revised: 29 December 2022

Accepted: 11 January 2023

Published: 13 January 2023



Copyright: © 2023 by the authors. Licensee MDPI, Basel, Switzerland. This article is an open access article distributed under the terms and conditions of the Creative Commons Attribution (CC BY) license (<https://creativecommons.org/licenses/by/4.0/>).

1. Introduction

Among terrestrial carbonates (calcareous tufa, stromatolitic tufa, and travertines), calcareous tufa represents a good proxy-indicator of Quaternary climatic and environmental conditions [1–7], widely observed in fluvial areas with calcareous deposits [8]. As tufas are mainly comprised of calcite, they enable direct and precise dating as well as geochemical reconstructions of the past geological environment [7]. Currently, such tufas are being used as a proxy for paleoclimate, paleohydrology, tectonic activity, glaciation, regional geomorphic evolution, human activity, and geoarchaeology studies [2,9–16]. Andrews et al. [2] reviewed paleoclimate records of riverine tufas using stable isotopes, and proposed a synthesis. Tye et al. [17] studied the Long Lake sequence of Marks Tey, Essex, UK, and showed that the $\delta^{18}\text{O}$ record of the endogenic carbonates from this sequence records the climatic structure of MIS 11. Matsuoka et al. [18] performed high-resolution stable isotopic analyses of an annually laminated tufa from Shirokawa, SW Japan. Zidi et al. [19] argued that the calcareous tufas of Boulaaba are good indicators of tectonic activity, as they are intimately related to the fault network distribution in the region. Tufa is deposited in open ground-surface environments, which leads to a complex deposition mechanism. Therefore,

how to accurately use tufa to reconstruct paleoclimate environment still needs a lot of in-depth research [20].

A large amount of tufa with different genetic types is distributed on the Tibetan Plateau [21]. On the eastern margin of the Tibetan plateau, there is a belt-shaped tufa area from northeast to southwest [22], and its distribution area is mainly located at the turning point before the top of the largest topographic step in the eastern Tibetan Plateau. The regional tufa mainly develops in the periglacial landform area at the lower part of the snow line [23,24]. Because of the special geographical location of the Tibetan Plateau, the tufa in this area is strongly indicative of paleoclimate and paleoenvironment [20,25–30]. Mischke et al. [31] identified the Mid-Holocene tufa section at an altitude of 3815 m in the Qilian Mountains at the northeastern margin of the Tibetan Plateau as a new and possibly important climate archive. Guo et al. [32] reconstructed regional paleoclimatic and paleohydrological changes during the Early and Mid-Holocene by analyzing the rhythmic nature and hydrochemical proxies of tufa in Jiuzhaigou, eastern Tibetan Plateau. Lei et al. [33] discussed the characteristics of major geochemical elements and paleoenvironmental significance of tufa deposited on the ancient lakeshore terrace of the Ngangla Ringsto Lake in the western Tibetan Plateau. Niu et al. [22] and Wang et al. [20] summarized previous studies on the geological information recorded by travertine and tufa on the Tibetan Plateau and proposed the prospect of future studies.

The Jiuzhaigou deposits are typical examples of calcareous tufa with the highest altitude (2200–2900 m) in the world. Jiuzhaigou calcareous tufas are porous deposits containing plants and algal molds or imprints [16,34,35]. The Jiuzhaigou Tufa Scenic Spot, a World Natural Heritage Site (Aba Tibetan and Qiang Autonomous Prefecture, China), is particularly interesting because of its spectacular large-scale plateau tufa lakes, tufa waterfalls, tufa beach flows, and other landforms. On 8 August 2018, an Mw 7.0 earthquake (hereinafter referred to as the “8.8 earthquake” based on the date) occurred in Jiuzhaigou, China. Following the earthquake, many new calcareous tufa profiles were revealed, such as the Nuorilang Waterfall and Sparkling Lake. Before the earthquake, there was a tufa calcareous dam (locally called the Yanacuo Dam) between the Sparkling Lake and the downstream Double-Dragon Lake. The earthquake caused the dam to break in the central part and exposed a rhythmic structure section. Based on mineral composition, thin section observation, major/trace element content, and stable isotope composition ($\delta^{13}\text{C}_{\text{V-PDB}}$, $\delta^{18}\text{O}_{\text{V-SMOW}}$), combined with previous scholars’ research results on calcareous tufa and Jiuzhaigou area, this paper analyzes the mechanism of calcareous tufa deposition in Jiuzhaigou and the influencing factors during the deposition process, and further discusses the geological environment that may be recorded by calcareous tufa deposition.

2. Geographic Setting

The Jiuzhaigou Natural Heritage Scenic Area in Sichuan Province, China (32°54′–33°19′ N, 103°46′–104°14′ N) is located in the conjunction of the Songpan–Ganzi orogenic belt and West Qinling orogenic belt (Figure 1a). The main faults in the surrounding area are the Tazang, Huya, Xueshanliangzi, and Minjiang faults (Figure 1b). The geological structure of the Jiuzhaigou region is complex, with strong neotectonic activity, fold-fault development, and frequent earthquakes (Figure 1b,c). The structural pattern of the scenic spot controls the geomorphological framework in the area and the structural lineaments are mainly distributed in the NW-SE direction (Figure 1c).

Owing to the vulnerability of the aquifer in the Jiuzhaigou area, after it is broken under the action of tectonic stress, rock joints and fractures in the fault are developed, with NW trending dominant directions, which conditions for the formation of a fissure crack. The interaction of groundwater infiltration and rock promotes the further expansion of fissures. In addition, the growth of fissures intensifies the infiltration and circulation of groundwater, alternately, and the fissure–karst process is mutually reinforcing, thereby accelerating the karst process. Identified through a field geological survey and the investigation report of the Sichuan Bureau of Geology and Mineral Resources, the lithofacies of the outcrop strata

in the Jiuzhaigou Scenic Spot are marine facies, and the lithology is mainly carbonate rocks, ranging in age from the Paleozoic Devonian to the Mesozoic Triassic. Various limestones (including bioclastic limestone, crystalline limestone, argillaceous limestone, and siliceous limestone) and trace amounts of dolomite, slate, and sandstone constitute the material basis of the Jiuzhaigou karst underground runoff system.

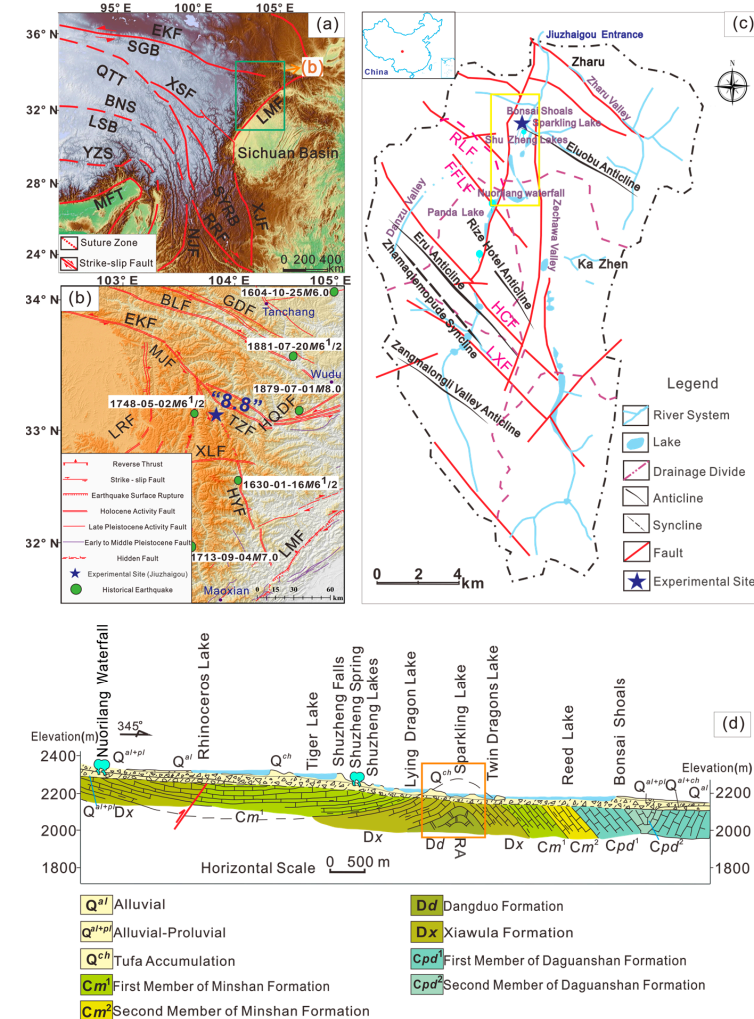


Figure 1. Geological background map of study area. (a) Regional tectonic geological map [36]. EKF = East Kunlun fault; XSF = Xianshuihe fault; QTT = QiangTang terrane; BNS = Bangong-Nujiang suture; LSB = Lhasa block; YZS = Yarlung-Zangbo suture; MFT = main frontal thrust; NJF = Nujiang fault; RRF = Red River fault; SYRB = Sichuan-Yunnan rhombic block; XJF = Xi-aojiang fault; LMF = Longmenshan fault; SGB = Songpan-Ganzi Block. The green frame is the area in (b). (b) Regional structure and distribution of magnitude $M \geq 6.0$ earthquakes in the Jiuzhaigou vicinity between 1630 and 1900 [37]. The blue frame shows the location of the Jiuzhaigou Scenic Spot. GDF = Guanggaishan-Dieshan fault; BLF = Bailongjiang fault; EKF = East Kunlun fault; MJF = MinJiang fault; TZF = Tazang fault; XLF = Xueshanliangzi fault; LMF = Longmenshan fault; HYF = Huya fault; LRF = Longriba fault; HQDF = Hanan-Qingshanwan-Daoqizi fault. The blue five-pointed star is the epicenter of the “8.8” earthquake. (c) Outline of the geological structure of the Jiuzhaigou Scenic Spot (from Sichuan Provincial Regional Geological Survey Team 2006). The yellow frame shows the location of Shuzheng Valley. The location of Sparkling Lake is indicated by a blue five-pointed star. LXF = Long Lake-XuanquanValley Fault; HCF = Hawk Claw Fault; FFLF = Five Flower Lake Fault; RLF = Rhinoceros Lake Fault. (d) Schematic of the Shuzheng Valley geological profile [38]. RA = Russian Anticline. The orange frame shows the location of the Sparkling Lake in the Shuzheng Valley profile.

The Jiuzhaigou Scenic Spot is distributed in a “Y” shape, with the Shuzheng Valley at the lower branch of the “Y” (Figure 1c). The elevation of the Shuzheng Valley is between 2210 m and 2250 m, and the total length from Entrance to Nuorilang is 13.8 km (Figure 1d). The Jiuzhaigou Scenic Spot has 30 small lakes, including the Sparkling Lake, Lying Dragon Lake, Five Flower Lake, Shuzheng lakes, and so on. The “8.8” earthquake caused serious damage to the two core scenic spots of Jiuzhaigou: the Nuorilang Waterfall and Sparkling Lake. The earthquake caused part of the viewing platform of the Nuorilang Waterfall to collapse. At the downstream of the Shuzheng Valley, the Sparkling Lake burst, forming a trapezoidal gap with a length of approximately 40 m, width of 12 m, and height of 15 m [39] (Figure 2a). The Sparkling Lake dried up almost completely after the “8.8” earthquake, and the calcareous tufa reef and calcareous tufa mound at the bottom of the lake were exposed. Following the collapse of the Sparkling Lake, a layered calcareous tufa profile with a recognizable rhythmic structure was revealed. The exposed profile has clear layers and a continuous deposition (Figure 2b), the color of the layers was mainly off-white, and black peat layers of considerable thickness were sandwiched (Figure 2b,c). The Sparkling Lake calcareous tufa profile provides a good experimental material for this study.

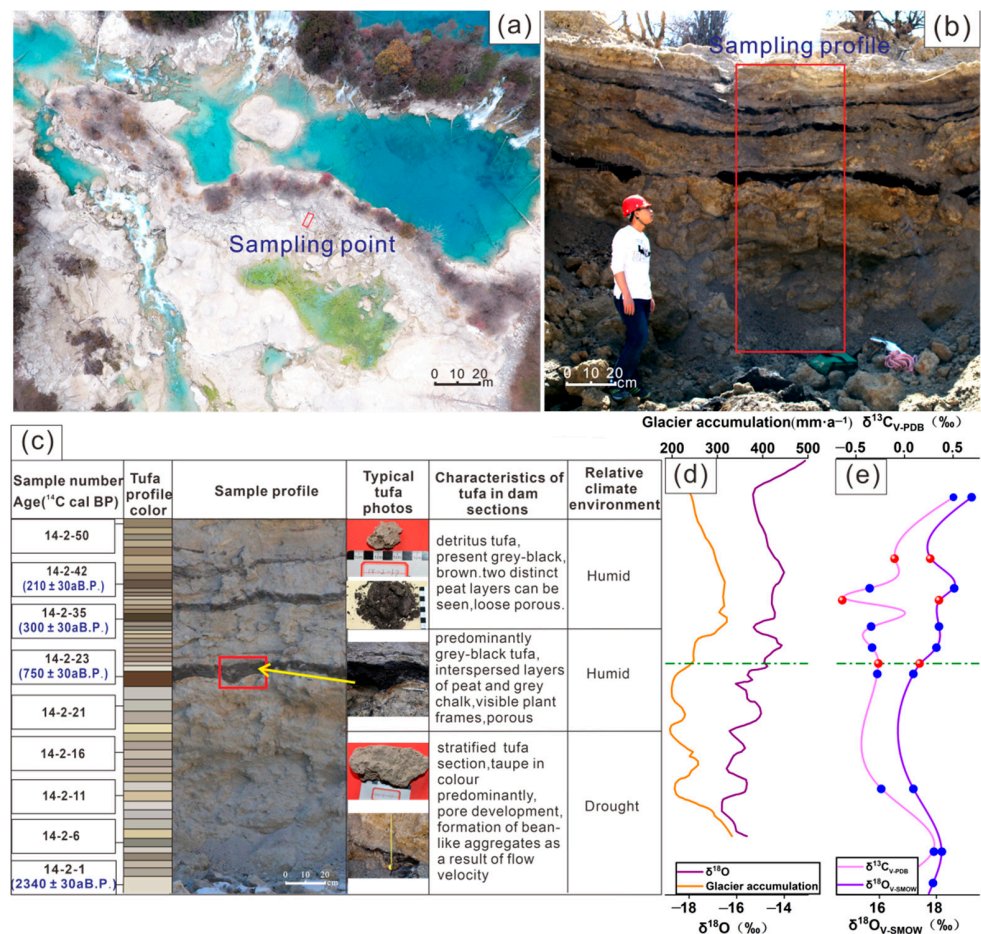


Figure 2. Collected calcareous tufa deposition profile at the Sparkling Lake. (a) The lake dried up after the earthquake. The red frame shows the sampling location. (b) Sparkling Lake calcareous tufa sampling profile. (c) Calcareous tufa characteristics and dating data. (d) Changes in ^{18}O and glacier accumulation recorded by Guliya ice cores over the last millennium (data from Yao et al. [40]). (e) Carbon-oxygen isotope analysis of the calcareous tufa profile. The blue dots represent experimentally measured carbon-oxygen isotope data. The red dots represent the location of the black peat layer.

3. Materials and Methods

3.1. Sample Collection

After the “8.8 earthquake”, the Sparkling Lake essentially dried up (Figure 2a). This study chose the fully exposed and partially collapsed central dam as the research object (Figure 2b). To obtain a fresh sample, the outermost layer of the profile was removed, and a steel pipe with a knife edge was used to knock in the calcareous tufa layer perpendicular to the section. According to the color variation, hardness, and structural characteristics of the calcareous tufa section, the samples are continuously and unevenly stratified from bottom to top. The bit distribution and thickness were marked, and the calcareous tufa sample was put into a clean cotton sample bag for coded storage. A sample was collected from each calcareous tufa layer, with each sample weighing approximately 2 kg. In total, 50 samples were collected, which were recorded as 14-2-1~14-2-50; the codes recorded on the three black peat layers were 14-2-23, 14-2-35, and 14-2-42 (Figure 2c).

Through the field geological survey, we observed and measured the formation occurrence and calcareous tufa profile of the strata in the study area. Further, we determined the attitude of rock formation and structural characteristics of the calcareous tufa. The collected samples were brought to the laboratory for analysis. Based on the establishment of the fine depositional time series of the calcareous tufa profile, the depositional environment changes of calcareous tufa in different periods are analyzed systematically, and the controlling factors affecting the change in depositional environment are also expounded.

3.2. Analytical Methods

The mineral phase analysis of calcareous tufa was completed at the Analytical Testing Center, Southwest University of Science and Technology (Mianyang, China), using an X-ray diffractometer (X'Pert Pro, PANalytical B.V.) under the following conditions: a copper target, 40 kV pipe pressure, 40 mA pipe flow, 0.033° step length, 0.2 °/min integration time, and 3–80 scan range. The stable isotope ($\delta^{13}\text{C}_{\text{V-PDB}}$, $\delta^{18}\text{O}_{\text{V-SMOW}}$) and major/trace element analysis of calcareous tufa was conducted by the ALS Laboratory Group (Guangzhou, China). The major elements of the rock were analyzed by the X-ray fluorescence spectrometer melting method. The rare earth trace elements were analyzed by an agilent inductively coupled plasma-optical emission spectrometer. Carbon-oxygen isotope analysis was conducted using a Thermo Finnigan Delta^{plus} XP isotope mass spectrometer. The measured results of $\delta^{13}\text{C}$ (precisions of 0.1‰, V-PDB standardization) and $\delta^{18}\text{O}$ (precisions of 0.5‰, V-SMOW standardization) are expressed in ‰. Radiocarbon dating was conducted on the calcareous tufa samples and performed at the BETA Laboratory (Miami, FL, USA) in accordance with ISO/IEC 17025:2017. The IntCal20 calibration curve was used. To eliminate the influence of “dead carbon”, the dating results were calibrated based on the precise dating of carbon in peat layers in the profile. The thin section observation was carried out in the Fundamental Science on Nuclear Wastes and Environmental Safety Laboratory of the Southwest University of Science and Technology (Mianyang, China). The instrument model is the Zeiss upright microscope Axio Scope A1. The technical parameters are as follows: the most advanced IC2S infinity axial, radial double chromatic aberration correction and contrast-enhanced optical system; the analyzer is 360° adjustable, the precision is 0.1°; the magnification is 50~500; and transmission, anti-bireflection light source.

4. Data Analysis

4.1. Calcareous Tufa Mineral Phase Test

Thirteen calcareous tufa samples with layers of different colors were selected for X-ray diffraction (XRD). The diffraction patterns of the obtained samples was compared and analyzed with the powder diffraction file (PDF) card using the MDI Jade 9.0 software. The results show that the diffraction peaks of the calcareous tufa samples are all well fitted with the calcite standard card (PDF#05-0586), indicating that the calcareous tufa was dominated by calcite (Figure 3). The peak position of calcite does not change considerably, with the strongest diffraction peak appearing at 29.4°. The diffraction peak baseline was flat, the peak

type was sharp, and the peak was obvious. The corresponding main dominant surfaces are {012}, {104}, {110}, {113}, {202}, {018}, {116}, {122}. After the qualitative information of the mineral is obtained, the Rietveld full-spectrum fitting method is used for semi-quantitative analysis to determine the content of mineral components in calcareous tufa samples of different colors. The analysis results are shown in Table 1. The samples of the Sparkling Lake calcareous tufa profile are shown to contain calcite and quartz. From the 14-2-23 sample upward, the calcite content basically dropped to below 90% and other mineral components appeared (such as Albite, Muscovite, Montmorillonite, and Kaolinite). Table 1 shows that the percentages of calcite in the three sets of black peat calcareous tufa layers are 4.8, 45.9, and 65.8, which are significantly lower than the percentages of about 80 in the gray-brown layers. Silicate minerals are present in all three sets of black peat layers. The content of Muscovite (43.8%) in sample 14-2-23 was even higher than that of calcite.

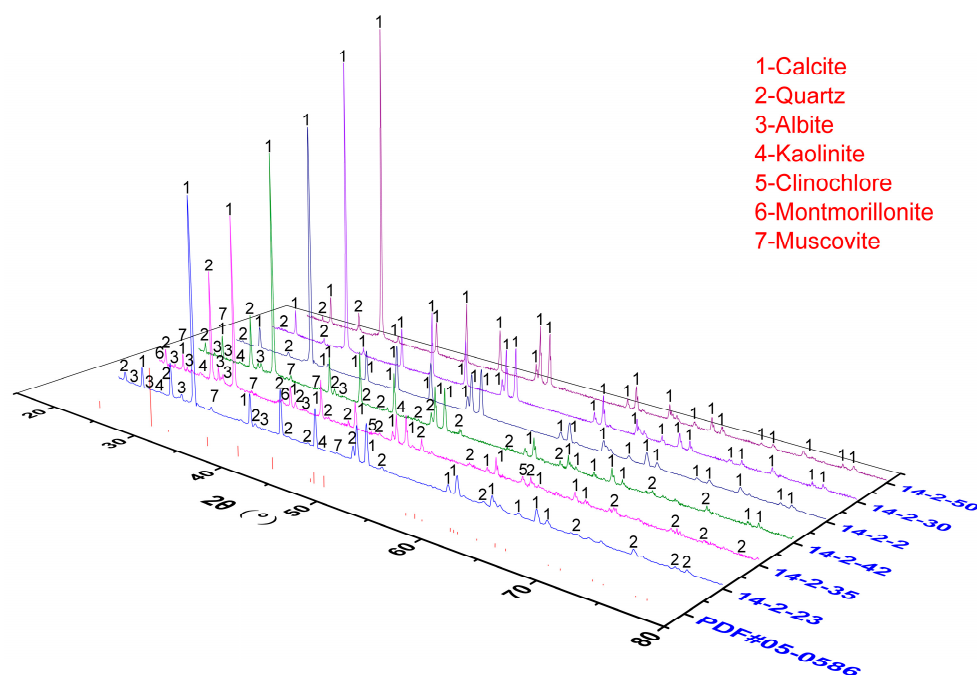


Figure 3. XRD patterns of calcareous tufa profile in Sparkling Lake.

Table 1. Mineral percentage of calcareous tufa profile in Sparkling Lake.

Sample Number	Quartz (%)	Calcite (%)	Clinochlore (%)	Albite (%)	Muscovite (%)	Montmorillonite (%)	Kaolinite (%)
14-2-2	1.8	98.2	-	-	-	-	-
14-2-4	2.0	98	-	-	-	-	-
14-2-5	4.4	95.6	-	-	-	-	-
14-2-11	1.8	98.2	-	-	-	-	-
14-2-22	3.4	96.6	-	-	-	-	-
14-2-23	27.5	4.8	10.8	3.3	43.8	4.6	5.2
14-2-26	8.9	74.3	-	0.4	11.6	-	4.8
14-2-30	2.1	97.9	-	-	-	-	-
14-2-34	5.3	93.2	-	1.5	-	-	-
14-2-35	20.9	45.9	4.7	3.8	19.1	1.8	3.8
14-2-37	3	81.1	-	-	9.4	-	6.5
14-2-42	11.7	65.8	-	1.6	18.3	-	2.6
14-2-50	4.1	95.9	-	-	-	-	-

4.2. Calcareous Tufa Radiocarbon Dating

The chemical index of alteration (CIA), an important index to evaluate the weathering history of sediments, is defined as $Al_2O_3 / (Al_2O_3 + CaO^* + Na_2O + K_2O) \times 100$, where the oxide is the molar mass percentage and CaO^* is only CaO in silicate [41–43]. Because of the difficulty in accurately separating silicate minerals in the sample, the correction method proposed by McLennan [44] was used to calculate the CIA value. Correlation analysis refers to the measurement of the degree of correlation between variable elements [45,46]. Here, Pearson correlation analysis was performed on the stable isotopes and major/trace elements using the IBM SPSS Statistics 25 software, which intuitively reflected the dependence and correlation degree of each indicator.

The lowest layers and three sets of black peat layers of the calcareous tufa profile were selected for radiocarbon dating. The age of the calcareous tufa profile of the Sparkling Lake was measured to be 2340 ± 30 – 210 ± 30 a.B.P. (Figure 2c), belonging to the Late Holocene. Combined with the warm–humid climate corresponding to the CIA value (60–80) (Table 2), this indicates that the calcareous tufa is the product of deposition in the warm–humid climate of the Late Holocene. Based on the superposition relationship and occurrence measured in the field, the Sparkling Lake calcareous tufa dam shows a bottom-up sequence from old to new, with sedimentary continuity, and the ^{14}C apparent age data are consistent, enabling a more detailed chronological sequence for the calcareous tufa deposition in Jiuzhaigou Scenic Spot.

Table 2. Content and ratios of major/trace elements in calcareous tufa of Sparkling Lake.

Sample Number	K (%)	Na (%)	Ca (%)	Mg (%)	Al (%)	K/Ca	K/Al	Na/Al	Mg/Al	Ca/Al	Al ₂ O ₃ (%)	K ₂ O (%)	Na ₂ O (%)	CaO (%)	MgO (%)	CIA
14-2-1	0.05	0.06	38.5	0.24	0.19	0.13	0.26	0.32	1.26	202.63	0.32	0.07	0.08	54.0	0.37	58.18
14-2-2	0.09	0.07	37.5	0.25	0.32	0.24	0.28	0.22	0.78	117.19	0.57	0.11	0.09	52.8	0.42	66.28
14-2-3	0.09	0.07	38.5	0.26	0.31	0.23	0.29	0.23	0.84	124.19	0.53	0.11	0.09	53.7	0.42	64.63
14-2-4	0.17	0.07	37.0	0.28	0.61	0.46	0.28	0.11	0.46	60.66	1.14	0.21	0.09	52.1	0.48	74.51
14-2-5	0.21	0.09	36.9	0.30	0.75	0.57	0.28	0.12	0.40	49.20	1.37	0.26	0.12	50.6	0.50	73.26
14-2-6	0.15	0.07	38.1	0.27	0.53	0.39	0.28	0.13	0.51	71.89	0.97	0.18	0.09	52.4	0.43	72.93
14-2-7	0.09	0.06	37.6	0.25	0.30	0.24	0.30	0.20	0.83	125.33	0.56	0.11	0.08	53.7	0.42	67.47
14-2-8	0.16	0.07	36.9	0.28	0.55	0.43	0.29	0.13	0.51	67.09	1.03	0.19	0.09	52.4	0.47	73.57
14-2-9	0.26	0.09	35.3	0.31	0.98	0.74	0.27	0.09	0.32	36.02	1.81	0.31	0.12	50.2	0.51	76.69
14-2-10	0.18	0.08	36.9	0.29	0.71	0.49	0.25	0.11	0.41	51.97	1.27	0.22	0.11	51.7	0.48	74.27
14-2-11	0.12	0.07	38.8	0.28	0.48	0.31	0.25	0.15	0.58	80.83	0.85	0.15	0.09	53.1	0.45	72.03
14-2-12	0.64	0.16	31.7	0.45	2.55	2.02	0.25	0.06	0.18	12.43	4.76	0.77	0.22	42.7	0.75	79.73
14-2-13	0.22	0.08	36.8	0.29	0.85	0.60	0.26	0.09	0.34	43.29	1.53	0.26	0.11	50.9	0.48	76.12
14-2-14	0.16	0.07	35.7	0.27	0.61	0.45	0.26	0.11	0.44	58.52	1.13	0.20	0.09	52.4	0.46	74.83
14-2-15	0.27	0.09	35.9	0.30	0.92	0.75	0.29	0.10	0.33	39.02	1.73	0.32	0.12	50.3	0.50	75.55
14-2-16	0.26	0.09	35.7	0.31	0.91	0.73	0.29	0.10	0.34	39.23	1.61	0.31	0.12	50.0	0.51	74.54
14-2-17	0.13	0.07	36.2	0.26	0.45	0.36	0.29	0.16	0.58	80.44	0.83	0.16	0.09	52.0	0.43	70.94
14-2-18	0.09	0.06	37.7	0.24	0.31	0.24	0.29	0.19	0.77	121.61	0.54	0.11	0.08	53.3	0.39	66.67
14-2-19	0.17	0.08	36.8	0.26	0.57	0.46	0.30	0.14	0.46	64.56	1.04	0.20	0.11	51.7	0.43	71.23
14-2-20	0.23	0.08	36.0	0.28	0.78	0.64	0.29	0.10	0.36	46.15	1.43	0.27	0.11	50.7	0.47	74.48
14-2-21	0.15	0.07	37.6	0.26	0.51	0.40	0.29	0.14	0.51	73.73	0.92	0.18	0.09	52.5	0.43	71.88
14-2-22	0.35	0.09	33.9	0.30	1.21	1.03	0.29	0.07	0.25	28.02	2.27	0.43	0.12	48.7	0.51	77.21
14-2-23	1.06	0.35	4.64	0.62	3.52	22.84	0.30	0.10	0.18	1.32	7.47	0.70	0.47	6.80	1.14	76.30
14-2-24	0.60	0.23	28.8	0.40	1.98	2.08	0.30	0.12	0.20	14.55	3.74	0.80	0.31	41.5	0.69	73.91
14-2-25	0.67	0.34	28.4	0.45	2.24	2.36	0.30	0.15	0.20	12.68	4.17	0.63	0.46	39.2	0.78	70.80
14-2-26	0.52	0.23	30.1	0.40	1.75	1.73	0.30	0.13	0.23	17.20	3.23	0.34	0.31	42.5	0.69	72.10
14-2-27	0.28	0.11	34.3	0.33	0.96	0.82	0.29	0.11	0.34	35.73	1.81	0.24	0.15	49.5	0.56	73.88
14-2-28	0.20	0.07	36.1	0.30	0.67	0.55	0.30	0.10	0.45	53.88	1.22	0.20	0.09	51.2	0.48	74.39
14-2-29	0.16	0.07	37.5	0.29	0.55	0.43	0.29	0.13	0.53	68.18	0.99	0.26	0.09	52.3	0.48	72.26
14-2-30	0.22	0.08	36.3	0.30	0.76	0.61	0.29	0.11	0.39	47.76	1.39	0.70	0.11	51.2	0.51	74.33
14-2-31	0.29	0.10	34.1	0.31	1.00	0.85	0.29	0.10	0.31	34.10	1.88	0.35	0.13	49.2	0.53	75.50
14-2-32	0.26	0.10	35.8	0.31	0.90	0.73	0.29	0.11	0.34	39.78	1.64	0.31	0.13	50.3	0.53	74.21
14-2-33	0.27	0.09	36.2	0.32	0.95	0.75	0.28	0.09	0.34	38.11	1.74	0.33	0.12	50.0	0.51	75.32
14-2-34	0.39	0.12	33.6	0.35	1.36	1.16	0.29	0.09	0.26	24.71	2.58	0.48	0.16	48.0	0.60	76.33
14-2-35	1.16	0.44	16.15	0.64	3.83	7.18	0.30	0.11	0.17	4.22	7.52	1.44	0.59	22.7	1.16	74.16
14-2-36	0.38	0.14	33.3	0.36	1.24	1.14	0.31	0.11	0.29	26.85	2.31	0.46	0.19	46.9	0.61	73.33
14-2-37	0.28	0.11	35.2	0.32	0.91	0.80	0.31	0.12	0.35	38.68	1.67	0.34	0.15	49.3	0.53	72.29
14-2-38	0.28	0.10	34.5	0.32	0.93	0.81	0.30	0.11	0.34	37.10	1.69	0.34	0.13	48.8	0.52	73.80

Table 2. Cont.

Sample Number	K (%)	Na (%)	Ca (%)	Mg (%)	Al (%)	K/Ca	K/Al	Na/Al	Mg/Al	Ca/Al	Al ₂ O ₃ (%)	K ₂ O (%)	Na ₂ O (%)	CaO (%)	MgO (%)	CIA
14-2-39	0.30	0.09	34.5	0.32	0.97	0.87	0.31	0.09	0.33	35.57	1.84	0.37	0.12	49.4	0.55	75.10
14-2-40	0.82	0.31	17.55	0.55	2.74	4.67	0.30	0.11	0.20	6.41	5.58	1.05	0.32	25.9	1.02	76.75
14-2-41	0.71	0.27	20.9	0.51	2.39	3.40	0.30	0.11	0.21	8.74	4.67	0.88	0.36	30.3	0.91	74.48
14-2-42	0.69	0.28	23.2	0.50	2.31	2.97	0.30	0.12	0.22	10.04	4.47	0.86	0.38	33.4	0.88	73.40
14-2-43	0.49	0.19	29.6	0.43	1.65	1.66	0.30	0.12	0.26	17.94	3.08	0.60	0.26	42.2	0.75	73.33
14-2-44	0.40	0.16	31.4	0.39	1.34	1.27	0.30	0.12	0.29	23.43	2.53	0.49	0.22	45.2	0.69	73.12
14-2-45	0.20	0.10	36.3	0.33	0.69	0.55	0.29	0.14	0.48	52.61	1.26	0.24	0.13	51.0	0.57	71.59
14-2-46	0.18	0.08	33.7	0.32	0.62	0.53	0.29	0.13	0.52	54.35	1.13	0.22	0.11	50.5	0.56	71.97
14-2-47	0.21	0.10	33.6	0.34	0.75	0.63	0.28	0.13	0.45	44.80	1.38	0.26	0.13	49.6	0.60	72.63
14-2-48	0.08	0.05	36.4	0.30	0.27	0.22	0.30	0.19	1.11	134.81	0.45	0.09	0.07	52.3	0.49	66.18
14-2-49	0.07	0.06	35.8	0.28	0.25	0.20	0.28	0.24	1.12	143.20	0.44	0.09	0.08	52.7	0.46	63.77
14-2-50	0.11	0.08	34.0	0.30	0.37	0.32	0.30	0.22	0.81	91.89	0.70	0.14	0.11	50.8	0.52	66.04

4.3. Thin Section Observation

In the thin-section results, lamellar limestone is evident in Figure 4a. The distribution side around the organic matrix is sparry calcite (Figure 4b–e). Outside, micrite and sparry calcite are distributed around the formed shell. Figure 4f shows sparry calcite and micrite around petioles. In the absence of organisms, there was a mix of micrite and sparry calcite around the void (Figure 4f). The void shape was irregular, which may be related to the recrystallization of micrite calcite. It is speculated that a microbial community exists in the litter accumulation and that the calcareous tufa is preferentially deposited by these organic matrices as a template. Around the organic matrices, bright crystal calcite is formed, and a cryptocrystalline structure dominated by muddy crystal is distributed around it. The calcareous tufa in Jiuzhaigou contains a large amount of algae and microorganisms (Figure 4g). Figure 4h shows the Sparkling Lake red algae population under the light microscope (400 times magnification). The thin-section results show that the tube bundle-shaped calcareous tufa formed by algal filaments and leaves as templates is dominated by splendid calcite on the inside and mainly micrite, microsparkle, and a mixture of the two on the outside. The difference of the crystal structures around the organic matrix indicates that the tubular channels were left during the decomposition of biomass from the inside to the outside. Further, there are gaps between the calcareous tufa inclusions formed by biological templates. In both cases, water flow with slow mobility passes through, which is conducive to recrystallization to form sparry calcite owing to excessive calcite saturation SiC (Figure 4i).

4.4. Results of the Major/Trace Element Analysis of Calcareous Tufa

From the calcareous tufa mineral composition analysis, the major/trace element contents in different color layers were further determined. The peaks of K, Ca, Na, Mg, Al, K/Ca, K/Al, and CIA in the calcareous tufa profile coincide with the black peat layers. In general, their peak values have a good correspondence with the black peat layers (Figure 5). The average values of K (0.97 g/kg), Na (0.36 g/kg), Mg (0.59 g/kg), Al (3.22 g/kg), K/Ca (10.00), K/Al (0.30), and CIA (74.62) in black peat layers were considerably higher than those in other color layers. Furthermore, the average value of Ca (14.66 g/kg) decreased considerably, about 20 g/kg (Table 2). Moreover, the Na/Al, Mg/Al, and Ca/Al peak values are diametrically opposite to the black peat layers (Figure 5). The average values of Na/Al (0.11), Mg/Al (0.19), and Ca/Al (5.19) were considerably lower (Table 2).

The deposition process of calcareous tufa mineral elements is affected by the changes in the geological environment. Therefore, a statistical analysis of major/trace elements can determine the correlation between calcareous tufa mineral elements and the possible origin of the elements. It was observed that the K in the calcareous tufa profile was considerably positively correlated with Na, Mg, Al, K/Ca, K/Al, and CIA ($p < 0.01$) (Table 3 and Figure 6), with a correlation coefficient greater than 0.5, and the variation trend was the closest. This indicates similar sources of the four elements, i.e., silicate minerals, which often occur in

soil. Ca showed a considerable negative correlation with K, Na, Mg, Al, CIA, K/Ca, and K/Al, indicating the dilution effect of other elements on Ca. A linear relationship between Al and K, Na, Ca, and Mg was observed, while Al has an exponential relationship with the CIA (Figure 6). These chemical element indexes provide important data for distinguishing different colors of calcareous tufa layers. The results show that the three black peat layers of the calcareous tufa profile have the characteristics of low Ca content and Na/Al, Mg/Al, and Ca/Al ratios, and higher levels of K, Na, Mg, Al, K/Ca, K/Al, and CIA.

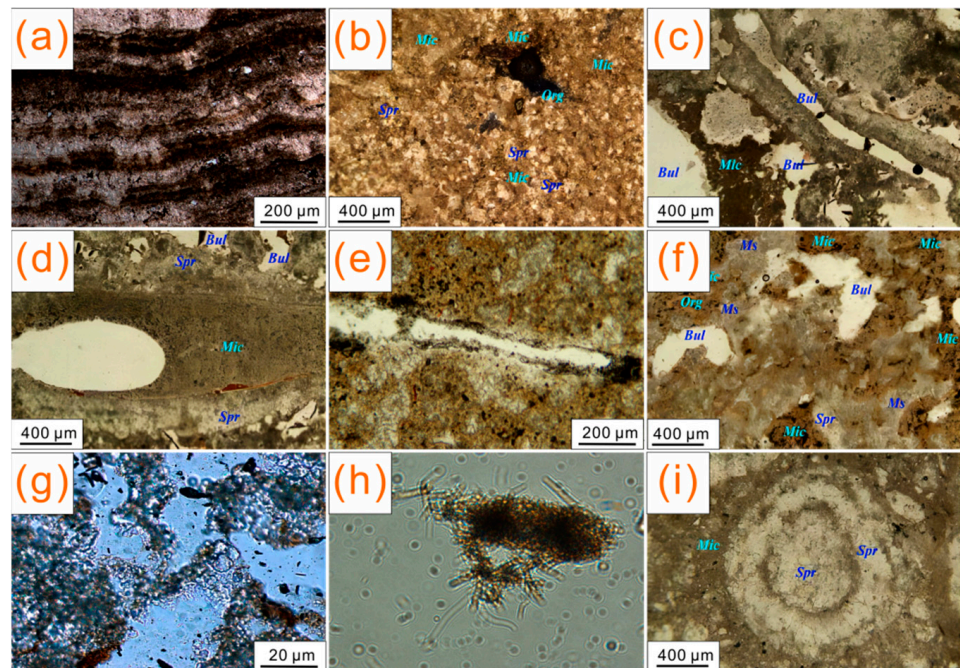


Figure 4. Thin-section results of Sparkling Lake calcareous tufa sample. (a) Lamellar limestone. (b–d) Surrounding the organic matrix distribution side is sparry calcite. (e) Calcite sparry and micrite around petiole. (f) Around the void with no living organisms involved. (g,h) Sparkling Lake red algae population. (i) Recrystallization forms sparry calcite. Spr = sparry, Mic = micrite, Ms = microspar, Org = organic.

4.5. Calcareous Tufa Carbon-Oxygen Isotope Test

Three sets of black peat and seven sets of gray-brown calcareous tufa were selected for carbon-oxygen isotope testing (Table 4). The $\delta^{13}\text{C}_{\text{V-PDB}}$ values of the calcareous tufa samples range from -0.62‰ to 0.50‰ (average -0.17‰). The $\delta^{18}\text{O}_{\text{V-SMOW}}$ values are between 17.78‰ and 19.23‰ (average 18.15‰). The $\delta^{13}\text{C}_{\text{V-PDB}}$ values of calcareous tufa black peat layer range from -0.62‰ to -0.10‰ (average -0.36‰). The lowest $\delta^{13}\text{C}_{\text{V-PDB}}$ value of the 4-2-35 sample is -0.62‰ , corresponding to the second layer of black peat in the calcareous tufa profile. The $\delta^{18}\text{O}_{\text{V-SMOW}}$ values of calcareous tufa in black peat layer vary slightly in the range of 17.78‰ to 18.09‰ (average 17.94‰). The correlation diagram shows that $\delta^{18}\text{O}_{\text{V-SMOW}}$ has a weak positive correlation or no obvious correlation with $\delta^{13}\text{C}_{\text{V-PDB}}$ (Figure 6). The correlation coefficient $R^2 = 0.27$. Carbon-oxygen isotopes were weakly correlated with K, Na, Ca, Mg, Al, CIA, and their ratios (K/Ca, K/Al, Na/Al, Mg/Al, and Ca/Al) (Table 3 and Figure 6).

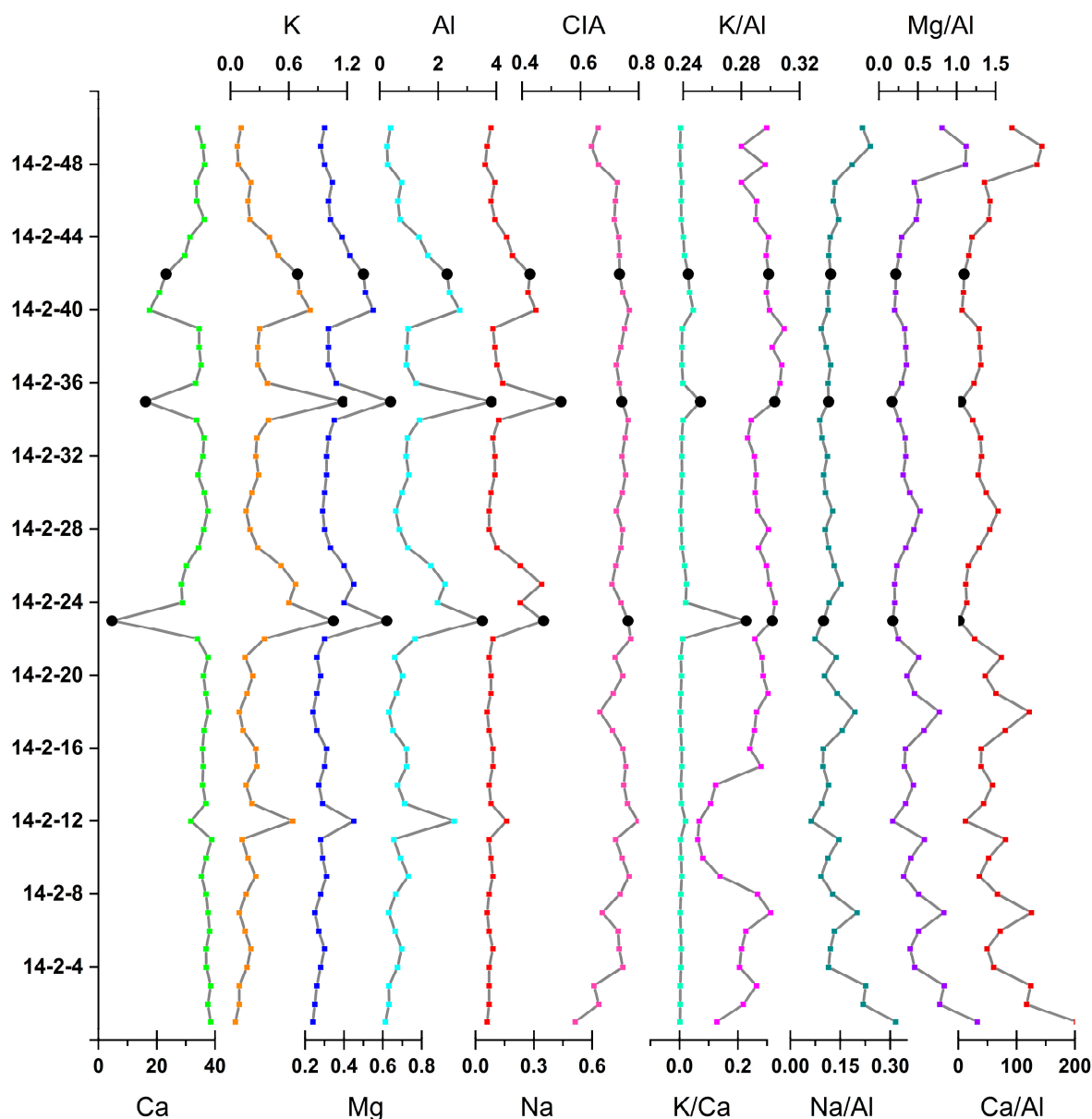


Figure 5. Element (Ca, K, Al, Na, Mg) composition content, element ratios (K/Ca, K/Al, Na/Al, Mg/Al, Ca/Al) and CIA value of calcareous tufa. The black dots indicate the location of the black peat layers.

Table 3. Pearson correlation matrix of main elements, element ratios, and isotopes ($\delta^{13}\text{C}_{\text{V-PDB}}$ and $\delta^{18}\text{O}_{\text{V-SMOW}}$) in the calcareous tufa profile.

Element	K	Na	Ca	Mg	Al	CIA	K/Ca	K/Al	Na/Al	Ca/Al	Mg/Al	$\delta^{18}\text{O}_{\text{V-SMOW}}$	$\delta^{13}\text{C}_{\text{V-PDB}}$
K	1												
Na	0.962 **	1											
Ca	-0.927 **	-0.905 **	1										
Mg	0.975 **	0.955 **	-0.954 **	1									
Al	0.997 **	0.949 **	-0.914 **	0.971 **	1								
CIA	0.467 **	0.284 *	-0.320 *	0.391 **	0.492 **	1							
K/Ca	0.727 **	0.670 **	-0.866 **	0.727 **	0.716 **	0.248	1						
K/Al	0.289 *	0.327 *	-0.333 *	0.279 *	0.231	-0.024	0.211	1					
Na/Al	-0.418 **	-0.237	0.261	-0.342 *	-0.437 **	-0.982 **	-0.195	-0.056	1				
Ca/Al	-0.722 **	-0.621 **	0.573 **	-0.671 **	-0.728 **	-0.869 **	-0.384 **	-0.231	0.865 **	1			
Mg/Al	-0.677 **	0.569 **	0.501 **	-0.594 **	-0.687 **	-0.890	-0.342 *	-0.180	0.880 **	0.980 **	1		
$\delta^{18}\text{O}_{\text{V-SMOW}}$	-0.238	-0.561 **	0.125	-0.144	-0.251	-0.561 *	-0.172	0.278	0.515	0.291	0.445	1	
$\delta^{13}\text{C}_{\text{V-PDB}}$	-0.529	0.046	0.384	-0.425	-0.529	-0.481	-0.506	-0.138	0.488	0.461	0.566 *	0.529	1

Note: * Correlation is considerable at $p < 0.05$ (two-tailed). ** Correlation is considerable at $p < 0.01$ (two-tailed).

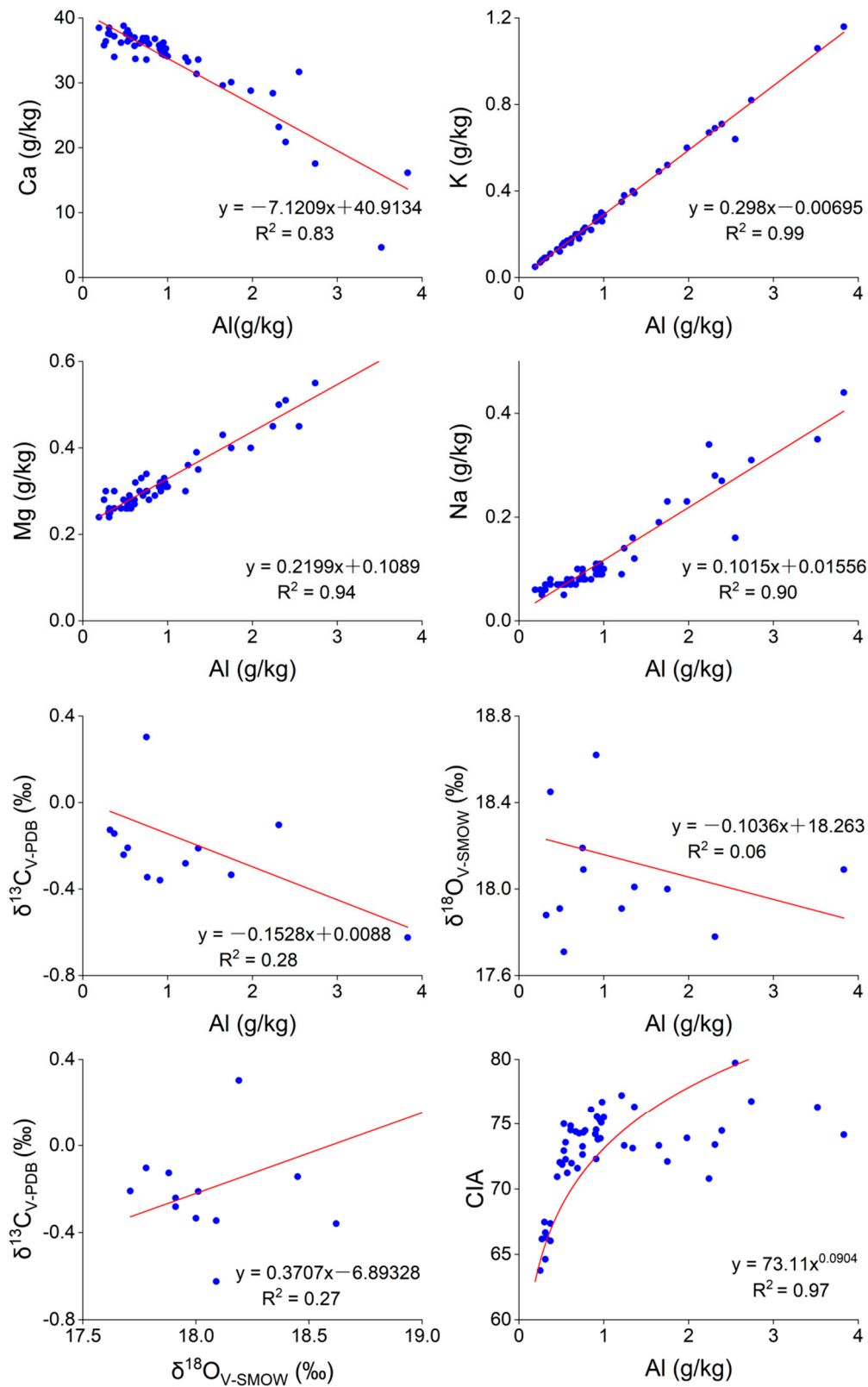


Figure 6. Correlation map of the main elements and carbon-oxygen isotopes of the calcareous tufa profile in the Sparkling Lake. It shows the correlation between elements (K, Na, Al, Mg, Ca, and CIA) and the plots of $\delta^{13}\text{C}_{\text{V-PDB}}$ and $\delta^{18}\text{O}_{\text{V-SMOW}}$.

Table 4. Carbon-oxygen isotope data of Sparkling Lake calcareous tufa profile.

Sample Number	$\delta^{13}\text{C}_{\text{V-PDB}}$ (‰)	$\delta^{18}\text{O}_{\text{V-SMOW}}$ (‰)
14-2-2	−0.13	17.88
14-2-5	0.30	18.19
14-2-11	−0.24	17.91
14-2-22	−0.28	17.91
14-2-23	the content of carbonate is low enough to measure C isotope	the content of carbonate is low enough to measure O isotope
14-2-26	−0.33	18.00
14-2-30	−0.35	18.09
14-2-34	−0.21	18.01
14-2-35	−0.62	18.09
14-2-37	−0.36	18.62
14-2-42	−0.10	17.78
14-2-50	0.50	19.23

5. Discussion

5.1. Response of Tufa Deposition to Paleohydrological Changes and Glaciation

Several authors have investigated the water source of the Jiuzhaigou Scenic Spot [38,47,48]. The Jiuzhaigou Scenic Spot is considered an independent karst hydrogeological structure unit where atmospheric precipitation (including atmospheric snowfall) is the only source of water supply. Therefore, isotope composition of the calcareous tufa in the study area reflects the changes in rainfall and temperature (Figure 2d,e). During 750 ± 30 – 300 ± 30 aB.P., the carbon isotope value of calcareous tufa showed a continuous decreasing trend. However, there is a weak positive correlation or no obvious correlation between carbon-oxygen isotopes in calcareous tufa (Table 3 and Figure 6), which is the same as the record of cave carbonate deposits in Southwest China [49,50]. Carbon-oxygen isotopes are consistent with precipitation and temperature changes recorded in the Guliya Ice Core [40] (before 750 ± 30 aB.P., it was a long cold and dry period, after which the precipitation and temperature showed a fluctuating upward trend) (Figure 2e). Carbon-oxygen isotopes records are consistent with the hydrological changes recorded in a compilation of 2000-year flood historical data in Sichuan [51]. Therefore, the analysis suggests that the information recorded by the calcareous tufa profile in the Sparkling Lake clearly reflects the heavy rainfall and the ablation of glaciers since the Holocene.

On the one hand, the isotope “dilution effect” caused by high rainfall conditions is extremely obvious in the Jiuzhaigou Valley [52–55]. That is, the light carbon isotope in the rain has played a “dilution role” in the heavy carbon isotope in calcareous tufa, making the carbon isotope in calcareous tufa lower. Before 750 ± 30 aB.P., the calcareous tufa carbon isotope values of Sparkling Lake were higher (average -0.09 ‰) (Table 4). It shows that the rainfall is relatively stable at this stage, and the water and soil are kept in good condition. At 750 ± 30 aB.P., the content of calcareous tufa carbonate dropped sharply, which was insufficient for the determination of carbon isotope. The content of calcite and Ca elements reached the lowest value (Tables 1 and 2). This period may result from flooding caused by heavy rains over a long period of time. After 750 ± 30 aB.P., the calcite and Ca contents decreased as a whole. However, the contents of other minerals and elements such as K, Na, Mg, and Al have increased to different degrees (Table 2 and Figure 5). The color of the calcareous tufa layers deepens, mainly to gray-black and brown (Figure 2b,c). The $\delta^{13}\text{C}_{\text{V-PDB}}$ value showed a decreasing trend. Around 300 ± 30 aB.P., the carbon isotope value reaches the lowest (-0.624 ‰) (Table 4). The occurrence of this phenomenon may be related to soil leaching. Heavy rainfall in the Jiuzhaigou area is speculated to have led to increased erosion; as a result, the water body that washed the soil carried large amounts of impurities (plants, organisms, minerals, and organic debris) (Figure 4). These impurity-carrying water bodies reduce the deposition rate of calcite and the increase in colored elements in its impurities, which makes the calcareous tufa layers at this stage

darker than the calcareous tufa formed in the cold and dry period, showing a gray-black or brown color. After 300 ± 30 aB.P., The $\delta^{13}\text{C}_{\text{V-PDB}}$ value continues to rise (Table 4). This indicates that rainfall decreases at this stage. At 210 ± 30 aB.P., a thinner layer of black peat appears. It is presumed to be related to the influence of tectonic activity or intensified human activity. During this period, vegetation was destroyed, soil erosion intensified, and the environment deteriorated.

On the other hand, the calcareous tufa in Jiuzhaigou was formed by multi-period accumulation. Previous studies suggested that the early tufas were accumulation landforms formed by alpine karstification in multiple periglacial environments [56,57]. Early tufa in Jiuzhaigou formed in a periglacial environment 520,000~30,000 years ago. After 30,000 years, the temperature in the region showed a fluctuating increase. Jiuzhaigou gradually withdrew from the periglacial environment. However, it was still covered by seasonal ice and snow. Currently, the runoff replenishment source of Jiuzhaigou is mainly rainfall, supplemented by seasonal snow melt water, which has obvious periodicity. However, the change in snow and ice is more sensitive to temperature than rainfall change, so ice and snow change has a better response to temperature change. Melting ice and snow increases free CO_2 in runoff, so the dissolution capacity is enhanced [58]. Part of the meltwater from ice and snow forms surface runoff and flows to the low-altitude Shuzheng Valley (Figure 1d). As water seeps further underground to become pore water, crevice water migrates along the fault direction. The strong dissolution of snowmelt runoff causes soil erosion, and the introduction of impurities such as soil particles and plant organic debris darkens the calcareous tufa layers (Figure 4). At the same time, the impurities deposited on the snow surface are washed out of the snow layer during the snowmelt period and migrate with the surface runoff and groundwater, which can replenish and dilute the elements in groundwater and surface water. The meltwater impurities contain more K, Na, Mg, and Al, which dilute the Ca content, affecting the elemental composition in the calcareous tufa layers (Table 2 and Figure 5). Due to the apparent isotopic fractionation during snow and ice melting, the light isotopic composition of the snow melt water is abundant [59], and the magnitude of contribution to the Jiuzhaigou Valley affects the stable isotope in the calcareous tufa. In summary, it can be concluded that the change in the meltwater flow of ice and snow caused by temperature changes directly or indirectly affects the deposition of calcareous tufa layers with different colors.

5.2. Response of Calcareous Tufa Deposition to Tectonic Activity

Calcareous tufa is highly sensitive to climate change. Therefore, calcareous tufas are often used as reliable climate proxies in many geological settings. Conversely, the research on the response of calcareous tufa to tectonic activity and earthquakes is rather limited. Pazzaglia et al. [60] concluded that the presence of calcareous tufas in the Ellera basin successfully allowed the disclosure of a wide array of paleoenvironmental and tectonic information and could be potentially extended to similar depositional contexts. The findings of Martini et al. [61] indicate that calcareous tufa deposits could serve as a sensitive proxy for tectonics when such deposits are associated with coarse-grained clastic deposits.

Jiuzhaigou is located in the transition zone of the deep and large fault zone, where tectonic activity is intense and earthquakes occur frequently (Figure 1a,b). Tufa development is closely related to this strong tectonic activity. Hence, calcareous tufa can be used to determine the occurrence time of faults or seismic activities and reveal more tectonic activity characteristics and evolution [20,22,23,62,63]. Three sets of black peat layers with a thickness of 5–20 cm developed in the calcareous tufa profile, aged 750, 300, and 210 ± 30 aB.P. Based on historical records [64,65], during the formation of the upper two sets of black peat layers, a series of large earthquakes of magnitude above 6.0 occurred around the area where Jiuzhaigou is located (Figure 1b). The analysis suggests that the formation of the black peat layers in the calcareous tufa profile may be related to strong seismic activities in the study area. The strong fault activity led to the fragmentation of underground rocks and the development of underground fractures and broken zones in

addition to inducing surface landslides and rock collapse and enhancing chemical weathering. The dissolution amount of the related minerals increased, affording an increase in K, Na, Mg, and Al contents in the black peat layers (Table 2 and Figure 5). Moreover, the strong tectonic activity triggered mountain collapse and soil erosion in the valleys, resulting in a large number of sources (broken rocks, vegetation, and particles of soil) mixed into the surface runoff. As a result, the hydrochemical environment was affected, and a large number of sources were accumulated during the deposition of calcareous tufa (Figure 4). Zheng et al. [66] compared the water chemistry and calcareous tufa deposition before and after the “8.8” earthquake in Jiuzhaigou, revealing the algal enrichment caused by enhanced soil erosion, which also caused the calcareous tufa deposits to become loose and porous. Moreover, the strong tectonic activity led to an abrupt change in the calcareous tufa deposition environment, the collapse of calcareous tufa dams, and the diversion of water bodies. A large amount of surface water leakage, aquatic algae death, the growth of airborne cyanobacteria, and weathering continues to increase, surface calcareous tufa will then disintegrate and desertification occurs, resulting in the loss of water and black calcareous tufa. The effects of strong earthquakes can persist for 10–20 years or more, after which calcareous tufa deposits enter the state of “normal deposits” (no longer affected by strong earthquakes to deposit) with a rhythmic structure. Dang et al. [67] and Qiao et al. [68] clarified that the “8.8” earthquake increased the degree of soil erosion and changed the water regulation effect of vegetation in the watershed. Soil erosion in the watershed has increased, a substantial number of sources such as sediment and wood have entered the body of water, and aquatic plants such as fir-leaf algae have grown in large numbers, resulting in turbid lakes and silted water bodies. Finally, the hydrochemical environment of calcareous tufa deposition is affected. Level changes as well as disappearances of groundwater in tectonically active regions due to earthquakes have been reported [69,70], suggesting that hydrological changes and depositional breaks in calcareous tufa in this area may also be caused by earthquakes. Qiu et al. [71] also proved the influence of the tectonic activity and earthquake on the Dawan travertine deposition in Huanglong (100 km away from the Jiuzhaigou Scenic Spot).

In summary, the formation of black peat layers in the calcareous tufa profile is the result of many factors caused by strong tectonic activity. Due to the lack of relevant studies on similar calcareous tufa profiles, a systematic comparative analysis cannot be conducted. Therefore, further studies are required to verify the above conclusions.

6. Conclusions

From the analysis of sedimentology, petrography and elemental geochemical characteristics of the differently colored layers of calcareous tufa in the Jiuzhaigou Scenic spot and ^{14}C dating results, combined with regional tectonic characteristics and geological environment changes, the following conclusions are drawn.

(1) The radiocarbon age of the calcareous tufa profile in the Sparkling Lake is 2340 ± 30 – 210 ± 30 aB.P. Therefore, the calcareous tufa of the Sparkling Lake belongs to the Late Holocene with a warm and humid climate. The sedimentary sequence of the calcareous tufa profile is the normal bottom-up sequence from old to new with good sedimentary continuity.

(2) Based on the dating results and geochemical analysis, it is believed that the deposition process of the calcareous tufa profile was controlled by paleoclimate and glaciation. The layers' color in the upper part of the tufa profile is significantly darker, suggesting a weak positive correlation of carbon-oxygen isotopes and the trend of change at or above centennial scale. The paleoclimate and glaciation changes reflected by these features are consistent with climate changes recorded in the ice cores on the Tibetan Plateau, carbonate cave deposits in Southwest China, and literature records. Therefore, this indicates that the information recorded in the calcareous tufa profile of the Sparkling Lake clearly reflects the heavy rainfall and the ablation of glaciers since the Holocene.

(3) The anomalous black peat layers in the calcareous tufa profile are related to strong regional tectonic activity (strong seismic activity). The ages of the three sets of black

peat layers in the upper part of the Sparkling Lake calcareous tufa profile are 750, 300, and 210 ± 30 aB.P., respectively, measured by ^{14}C dating. Among them, the ages of 300 and 210 ± 30 aB.P. are consistent with the time when a series of earthquakes with a magnitude above 6.0 occurred around Jiuzhaigou (1630~1900). The analysis shows that under the synergism effect of various factors caused by strong tectonic activities, the dissolution amount of related minerals is increased, and large amounts of vegetation, sediment, and other sources are mixed into the calcareous tufa for accumulation, affecting the hydrochemical environment of calcareous tufa deposition and forming a large amount of plant debris accumulation. In addition, strong tectonic activity led to the collapse of the calcareous tufa dam; moreover, water bodies were diverted, the calcareous tufa lost water and oxidized, the vegetation grew, and finally, black peat layers were formed.

Author Contributions: Conceptualization, C.L., X.Z. and F.W.; software, C.L., Y.J. and K.H.; validation, C.L., X.Z. and F.W.; formal analysis, C.L. and H.Z. (Hongmin Zhang); investigation, C.L., X.Z., Y.J., H.Z. (Hongmin Zhang) and F.W.; resources, X.Z., F.W. and Q.L.; data curation, C.L. and H.Z. (Hongmin Zhang); writing—original draft preparation, C.L. and H.Z. (Hongmin Zhang); writing—review and editing, C.L., X.Z., H.Z. (Heyan Zhu) and K.H.; visualization, C.L., Y.J. and H.Z. (Heyan Zhu); supervision, X.Z., F.W. and Q.L.; project administration, X.Z. and F.W.; funding acquisition, X.Z. and F.W. All authors have read and agreed to the published version of the manuscript.

Funding: This work was supported by the National Natural Science Foundation of China (grant nos. 41672206, 41973053, 42042030, U21A2016); the State Key Laboratory of Earthquake Dynamics, Institute of Geology, China Earthquake Administration (grant no. LED2016B07); and the Sichuan Province Overseas High-end Talent Introduction Project (grant no. 22RCYJ0060).

Data Availability Statement: Not applicable.

Acknowledgments: We greatly appreciate the help of the Jiuzhaigou Administration Bureau PetroChina for the fieldwork. We would also like to express our sincere gratitude to Qunwei Dai and Lanjie Hou from the Southwest University of Science and Technology for their helpful discussion and guidance on the early conception of this manuscript. Thanks are also owed to Lujia Yu for his help with the fieldwork and his comments in the process. Many thanks to the academic editors and the three peer reviewers for their constructive suggestions to improve the quality of the article.

Conflicts of Interest: The authors declare no conflict of interest.

References

1. Andrew, J.E.; Pedley, M.; Dennis, P.F. Palaeoenvironmental records in Holocene Spanish tufas; a stable isotope approach in search of reliable climatic archives. *Sedimentology* **2000**, *47*, 961–978. [[CrossRef](#)]
2. Andrews, J.E. Palaeoclimatic records from stable isotopes in riverine tufas: Synthesis and review. *Earth-Sci. Rev.* **2006**, *75*, 85–104. [[CrossRef](#)]
3. Viles, H.A.; Taylor, M.P.; Nicoll, K.; Neumann, S.; Nash, D.J.; Bullard, J.; North, C.P. Facies evidence of hydroclimatic regime shifts in tufa depositional sequences from the arid Naukluft Mountains, Namibia. *Sediment. Geol.* **2007**, *195*, 39–53. [[CrossRef](#)]
4. Bertini, A.; Minissale, A.; Ricci, M. Use of Quaternary travertines of central-southern Italy as archives of paleoclimate, paleohydrology and neotectonics. *Alp. Mediterr. Quat.* **2008**, *21*, 99–112.
5. Capezzuoli, E.; Gandin, A.; Sandrelli, F.; Pedley, H.M.; Rogerson, M. Calcareous tufa as indicators of climatic variability; a case study from southern Tuscany (Italy). *Geol. Soc. Spec. Publ.* **2010**, *336*, 263–281. [[CrossRef](#)]
6. Cremaschi, M.; Zerboni, A.; Spoetl, C.; Felletti, F. The calcareous tufa in the Tadrart Acacus Mt. (SW Fezzan, Libya); an early Holocene palaeoclimate archive in the central Sahara. *Palaeogeogr. Palaeoclimatol. Palaeoecol.* **2010**, *287*, 81–94. [[CrossRef](#)]
7. Dabkowski, J. High potential of calcareous tufas for integrative multidisciplinary studies and prospects for archaeology in Europe. *J. Archaeol. Sci.* **2014**, *52*, 72–83. [[CrossRef](#)]
8. Pentecost, A. The Quaternary travertine deposits of Europe and Asia Minor. *Quat. Sci. Rev.* **1995**, *14*, 1005–1028. [[CrossRef](#)]
9. Liu, Z.; Li, H.; You, C.; Wan, N.; Sun, H. Thickness and stable isotopic characteristics of modern seasonal climate-controlled sub-annual travertine laminas in a travertine-depositing stream at Baishuitai, SW China; implications for paleoclimate reconstruction. *Environ. Geol.* **2006**, *51*, 257–265. [[CrossRef](#)]
10. Luigi, D.F.; Claudio, F.; Andrea, B.; Erlisiana, A.; Mauro, B.; Michele, S.; Paola, T. Plateau versus fissure ridge travertines from Quaternary geothermal springs of Italy and Turkey: Interactions and feedbacks between fluid discharge, paleoclimate, and tectonics. *Earth Sci. Rev.* **2013**, *123*, 35–52. [[CrossRef](#)]
11. Gradzinski, M.; Wroblewski, W.; Dulinski, M.; Hercman, H.; Capezzuoli, E.; Capezzuoli, E. Earthquake-affected development of a travertine ridge. *Sedimentology* **2014**, *61*, 238–263. [[CrossRef](#)]

12. Kokh, S.N.; Sokol, E.V.; Deev, E.V.; Ryapolova, Y.M.; Rusanov, G.G.; Tomilenko, A.A.; Bul’Bak, T.A. Post-late glacial calcareous tufas from the Kurai fault zone (southeastern Gorny Altai, Russia). *Sediment. Geol.* **2017**, *355*, 1–19. [[CrossRef](#)]
13. Priestley, S.C.; Karlstrom, K.E.; Love, A.J.; Crossey, L.J.; Polyak, V.J.; Asmerom, Y.; Meredith, K.T.; Crow, R.; Keppel, M.N.; Habermehl, M.A. Uranium series dating of Great Artesian Basin travertine deposits: Implications for palaeohydrogeology and palaeoclimate. *Palaeogeogr. Palaeoclimatol. Palaeoecol.* **2017**, *490*, 163–177. [[CrossRef](#)]
14. Meyer, M.C.; Aldenderfer, M.S.; Wang, Z.; Hoffmann, D.L.; Dahl, J.A.; Degering, D.; Haas, W.R.; Schluetz, F. Permanent human occupation of the central Tibetan Plateau in the early Holocene. *Science* **2017**, *357*, 64–67. [[CrossRef](#)] [[PubMed](#)]
15. Andrea, S.; Paola, M.; Michele, S.; Paola, T.; Erlisiana, A.; Andrea, B.; Stefania, F.; Massimo, R.; Luca, T. The uplift of the Adriatic flank of the Apennines since the Middle Pleistocene: New insights from the Tronto River basin and the Acquasanta Terme Travertine (central Italy). *Geomorphology* **2020**, *352*, 106990. [[CrossRef](#)]
16. Wang, F.; Zhao, X.; Dong, F.; Enrico, C.; Alexander, I.M.; Du, J. Classification of Alpine-type travertine in Jiuzhaigou valley on the eastern margin of the Qinghai-Tibet Plateau. *Carsol. Sin.* **2021**, *40*, 112–124. [[CrossRef](#)]
17. Tye, G.J.; Sherriff, J.; Candy, I.; Coxon, P.; Palmer, A.; McClymont, E.L.; Schreve, D.C. The $\delta^{18}\text{O}$ stratigraphy of the Hoxnian lacustrine sequence at Marks Tey, Essex, UK: Implications for the climatic structure of MIS 11 in Britain. *J. Quat. Sci.* **2016**, *31*, 75–92. [[CrossRef](#)]
18. Matsuoka, J.; Kano, A.; Oba, T.; Watanabe, T.; Sakai, S.; Seto, K. Seasonal variation of stable isotopic compositions recorded in a laminated tufa, SW Japan. *Earth Planet. Sci. Lett.* **2001**, *192*, 31–44. [[CrossRef](#)]
19. Zidi, M.K.; Ben Ahmed, W.; Henchiri, M. Late Pleistocene Boulaaba travertine and calcareous tufa, Kasserine, Central Tunisia: Implications for North African spring-fed Ca-carbonates. *Quatern. Int.* **2022**, *637*, 57. [[CrossRef](#)]
20. Wang, Z.; Yin, J.; Yuan, D. Possibilities and problems associated with travertines and tufas in Quaternary studies: A case of the Tibetan Plateau. *Chin. Sci. Bull.* **2018**, *63*, 1012–1023. [[CrossRef](#)]
21. Geological Survey of China University of Geosciences. *The Instruction of Quaternary Geological and Geomorphologic Map of Qinghai-Tibetan Plateau and Its Adjacent Area*; Geological Survey of China University of Geosciences: Wuhan, China, 2010.
22. Niu, X.; Zheng, M.; Liu, X.; Qi, L. Sedimentary property and the geological significance of travertines in Qinghai-Tibetan Plateau. *Sci. Technol. Rev.* **2017**, *35*, 59–64.
23. Zhou, L. Characteristics of the Typical Hot Springs in the Central Tibet. Master’s Thesis, China University of Geosciences, Beijing, China, 2012.
24. Zhou, X. On Periglacial Karst in the Minshan Mountains. *Acta Geol. Sichuan* **2013**, *33*, 479–487.
25. Zentmyer, R.; Myrow, P.M.; Newell, D.L. Travertine deposits from along the South Tibetan Fault System near Nyalam, Tibet. *Geol. Mag.* **2008**, *145*, 753–765. [[CrossRef](#)]
26. Liu, Z.; Sun, H.; Baoying, L.; Xiangling, L.; Wenbing, Y.; Cheng, Z. Wet-dry seasonal variations of hydrochemistry and carbonate precipitation rates in a travertine-depositing canal at Baishuitai, Yunnan, SW China; implications for the formation of biannual laminae in travertine and for climatic reconstruction. *Chem. Geol.* **2010**, *273*, 258–266. [[CrossRef](#)]
27. Gao, J.; Zhou, X.; Fang, B.; Li, T.; Tang, L.; Catto, N. U-series dating of the travertine depositing near the Rongma Hot Springs in northern Tibet, China, and its paleoclimatic implication. *Quatern. Int.* **2013**, *298*, 98–106. [[CrossRef](#)]
28. Qin, J.; Han, P.; Che, X.; Yuan, G.; Fang, B.; Wang, G. Resuming the Holocene paleoclimate using $\delta^{18}\text{O}$ and trace elements of travertine in Rongma area, Tibet. *Earth Sci. Front.* **2014**, *21*, 312–322. [[CrossRef](#)]
29. Wang, Z.; Meyer, M.C.; Hoffmann, D.L. Sedimentology, petrography and early diagenesis of a travertine-colluvium succession from Chusang (southern Tibet). *Sediment. Geol.* **2016**, *342*, 218–236. [[CrossRef](#)]
30. Wang, Z.; Meyer, M.C.; Gliganic, L.A.; Hoffmann, D.L.; May, J. Timing of fluvial terrace formation and concomitant travertine deposition in the upper Sutlej River (Tirthapuri, southwestern Tibet) and paleoclimatic implications. *Quat. Sci. Rev.* **2017**, *169*, 357–377. [[CrossRef](#)]
31. Mischke, S.; Chengjun, Z. A laminated tufa carbonate from the mid Holocene of the Qilian Mountains and its potential for palaeoclimate inferences. *Episodes* **2008**, *31*, 401–407. [[CrossRef](#)]
32. Guo, Y.; Ge, Y.; Cui, P.; Chen, X.; Mao, P.; Liu, T.; Zhou, L. Early and mid-Holocene hydroclimate change recorded in tufa deposits in the Jiuzhaigou gully, eastern Tibetan Plateau. *Catena* **2021**, *196*, 104834. [[CrossRef](#)]
33. Lei, G.L.; Zhang, H.C.; Li, Z.Z.; Adam, M.H.; Zhu, Y.; Jiang, X.Y.; Chen, X.L.; Chang, F.Q.; Li, H.Y. Geochemical features and significance of shoreline tufa from a closed-basin lake ngangla ring tso in the western tibetan plateau. *Quat. Sci.* **2013**, *33*, 839–847. [[CrossRef](#)]
34. Florsheim, J.L.; Ustin, S.L.; Tang, Y.; Di, B.; Huang, C.; Qiao, X.; Peng, H.; Zhang, M.; Cai, Y. Basin-scale and travertine dam-scale controls on fluvial travertine, Jiuzhaigou, southwestern China. *Geomorphology* **2013**, *180–181*, 267–280. [[CrossRef](#)]
35. Lugli, S.; Tang, Y.; Reghizzi, M.; Qiao, X.; Schreiber, B.C.; Deng, G. Seasonal Pattern In the High-Elevation Fluvial Travertine From the Jiuzhaigou National Nature Reserve, Sichuan, Southwestern China. *J. Sediment. Res.* **2017**, *87*, 253–271. [[CrossRef](#)]
36. Bai, D.; Unsworth, M.J.; Meju, M.A.; Ma, X.; Teng, J.; Kong, X.; Sun, Y.; Sun, J.; Wang, L.; Jiang, C.; et al. Crustal deformation of the eastern Tibetan Plateau revealed by magnetotelluric imaging. *Nat. Geosci.* **2010**, *3*, 358–362. [[CrossRef](#)]
37. Yi, G.; Long, F.; Liang, M.; Zhang, H.; Zhao, M.; Ye, Y.; Zhang, Z.; Qi, Y.; Wang, S.; Gong, Y.; et al. Focal mechanism solutions and seismogenic structure of the 8 August 2017 M7.0 Jiuzhaigou earthquake and its aftershocks, northern Sichuan. *Chin. J. Geophys.* **2017**, *60*, 4083–4097.

38. Gan, J.; Liu, M.; Huang, R.; Fan, C.; Li, Q.; Wang, C. A study of hydrological cycle in the Jiuzhaigou core scenic area. *Hydrogeol. Eng. Geol.* **2010**, *37*, e39. [[CrossRef](#)]
39. Wang, D.; Zhou, Y.; Pei, X.; Ouyang, C.; Du, J.; Gianvito, S. Dam-break dynamics at Huohua Lake following the 2017 M_w 6.5 Jiuzhaigou earthquake in Sichuan, China. *Eng. Geol.* **2021**, *289*, 106145. [[CrossRef](#)]
40. Yao, T.; Qing, D.; Tian, L.; Jiao, K.; Yang, Z.; Xie, C.; Thompson, L.G. Changes of temperature and precipitation over the Qinghai-Tibet Plateau during the past 2ka—Guliya Ice Core record. *Sci. Sin. Terrae* **1996**, *26*, 348–353.
41. Nesbitt, H.W.; Young, G.M. Prediction of some weathering trends of plutonic and volcanic rocks based on thermodynamic and kinetic considerations. *Geochim. Cosmochim. Acta* **1984**, *48*, 1523–1534. [[CrossRef](#)]
42. Nesbitt, H.W.; Young, G.M. Formation and diagenesis of weathering profiles. *J. Geol.* **1989**, *97*, 129–147. [[CrossRef](#)]
43. Kautz, C.Q.; Martin, C.E. Chemical and physical weathering in New Zealand’s Southern Alps monitored by bedload sediment major element composition. *Appl. Geochem.* **2007**, *22*, 1715–1735. [[CrossRef](#)]
44. McLennan, S.M. Weathering and global denudation. *J. Geol.* **1993**, *101*, 295–303. [[CrossRef](#)]
45. Zhang, C.; Yang, B. *Fundamentals of Quantitative Geography*, 2nd ed.; Higher Education Press: Beijing, China, 2007; p. 202.
46. Xu, J. *Mathematical Methods in Contemporary Geography*, 3rd ed.; Higher Education Press: Beijing, China, 2017; p. 432.
47. Yin, G.; Fan, X.; Guo, J.; Yang, J. Isotope Tracer on Water Cycle System in Jiuzhaigou, Sichuan. *Acta Geogr. Sin.* **2000**, *55*, 487–494. [[CrossRef](#)]
48. Yin, G.; Ni, S.; Zhang, Q. Deuterium excess parameter and geohydrology significance—Taking the geohydrology researches in Jiuzhaigou and Yele, Sichuan for example. *J. Chengdu Univ. Technol.* **2001**, *28*, 251–254.
49. Dykoski, C.A.; Edwards, R.L.; Cheng, H.; Yuan, D.; Cai, Y.; Zhang, M.; Lin, Y.; Qing, J.; An, Z.; Revenaugh, J. A high-resolution, absolute-dated Holocene and deglacial Asian monsoon record from Dongge Cave, China. *Earth Planet. Sci. Lett.* **2005**, *233*, 71–86. [[CrossRef](#)]
50. Hu, C.; Henderson, G.M.; Huang, J.; Xie, S.; Sun, Y.; Johnson, K.R. Quantification of Holocene Asian monsoon rainfall from spatially separated cave records. *Earth Planet. Sci. Lett.* **2008**, *266*, 221–232. [[CrossRef](#)]
51. Changjiang Water Resources Commission of the Ministry of Water Resources. *Compilation of 2000-Year Flood Historical Data in Sichuan*; Cultural Relics Press: Beijing, China, 1993; p. 594.
52. Liu, Z.; Li, Q.; Sun, H.; Wang, J. Seasonal, diurnal and storm-scale hydrochemical variations of typical epikarst springs in subtropical karst areas of SW China: Soil CO_2 and dilution effects. *J. Hydrol.* **2007**, *337*, 207–223. [[CrossRef](#)]
53. Sun, H.; Liu, Z. Wet–dry seasonal and spatial variations in the $\delta^{13}C$ and $\delta^{18}O$ values of the modern endogenic travertine at Baishuitai, Yunnan, SW China and their paleoclimatic and paleoenvironmental implications. *Geochim. Cosmochim. Acta* **2010**, *74*, 1016–1029. [[CrossRef](#)]
54. Wang, H.; Yan, H.; Liu, Z. Contrasts in variations of the carbon and oxygen isotopic composition of travertines formed in pools and a ramp stream at Huanglong Ravine, China: Implications for paleoclimatic interpretations. *Geochim. Cosmochim. Acta* **2014**, *125*, 34–48. [[CrossRef](#)]
55. Yan, H.; Liu, Z.; Sun, H. Effect of in-stream physicochemical processes on the seasonal variations in $\delta^{13}C$ and $\delta^{18}O$ values in laminated travertine deposits in a mountain stream channel. *Geochim. Cosmochim. Acta* **2017**, *202*, 179–189. [[CrossRef](#)]
56. Li, H.; Zhou, X.; Li, G. Thermoluminescence age of sedimentary calcium carbonate in late geological history. *Chin. Sci. Bull.* **1988**, *33*, 775–778.
57. Dong, F. China’s travertine—the most natural asset in karst landscape worthy of world research and protection. *Carsol. Sin.* **2021**, *40*, 1–3.
58. Ocampo, J.; Klinger, J. Adsorption of N_2 and CO_2 on ice. *J. Colloid Interface Sci.* **1982**, *86*, 377–383. [[CrossRef](#)]
59. Qian, Z.; Yuan, Z.; Xu, J. Climatic characteristics of the last glacial period of Quaternary and Holocene climate recorded by oxygen and carbon isotopes in YaO2 hole, Yanhai, Yimeng, Inner Mongolia. *Geol. Chem. Miner.* **2002**, *24*, 96–100. [[CrossRef](#)]
60. Pazzaglia, F.; Barchi, M.R.; Buratti, N.; Cherin, M.; Pandolfi, L.; Ricci, M. Pleistocene calcareous tufa from the Ellera basin (Umbria, central Italy) as a key for an integrated paleoenvironmental and tectonic reconstruction. *Quatern. Int.* **2013**, *292*, 59–70. [[CrossRef](#)]
61. Martini, I.; Capezzuoli, E. Interdigitated fluvial clastic deposits and calcareous tufa testifying an uplift of the catchment area: An example from the Pianizzoli area (southern Tuscany, Italy). *Sediment. Geol.* **2014**, *299*, 60–73. [[CrossRef](#)]
62. Peng, G.; Jiao, W. Sedimentary age of travertine sinter in Jianchuan and new activity of Jianchuan fault. *J. Seismol. Res.* **1990**, *13*, 166–172.
63. Yuan, D.; Liu, Z.; Lin, Y.; Shen, J.; He, S.; Xu, S. *Karst Dynamical System in China*; Geology Press: Beijing, China, 2002; p. 275.
64. China Earthquake Administration. *Catalogue of Historical Strong Earthquakes in China*; Seismological Press: Beijing, China, 1995.
65. Sun, C. *Sichuan Earthquake Full Record*; Sichuan People’s Publishing House: Chengdu, China, 2010.
66. Zheng, X.; Tang, Y.; Du, J.; Lugli, S.; Xiao, Y.; Yang, Q.; Song, H.; Qiao, X. Enhanced soil erosion threatens fluvial tufa landscapes after an M_s 7.0 earthquake in the Jiuzhaigou World Heritage Site, southwestern China. *Sci. Total Environ.* **2022**, *848*, 157632. [[CrossRef](#)]
67. Dang, Z.; Ren, J.; An, C.; Dai, Q.; Dong, F.; Deng, Y.; Yang, Q.; Zhuo, M. Effect of M_s 7.0 earthquake on travertine landscapes and hydrochemistry of Jiuzhaigou core scenic spots. *Carsol. Sin.* **2019**, *38*, 186–192.
68. Qiao, X.; Xiao, Y.; Du, J.; Tang, Y.; Xiao, W.; Zheng, X.; Zhang, M. Tufa Landscapes in the Key Scenic Areas of the Jiuzhaigou Natural World Heritage Site: A critical Review and Future Research Needs. *Earth Environ.* **2022**, *50*, 202–218.

69. Hosono, T.; Yamada, C.; Shibata, T.; Tawara, Y.; Wang, C.Y.; Manga, M.; Rahman, A.T.M.S.; Shimada, J. Coseismic Groundwater Drawdown Along Crustal Ruptures During the 2016 Mw 7.0 Kumamoto Earthquake. *Water Resour. Res.* **2019**, *55*, 5891–5903. [[CrossRef](#)]
70. Ichiyanagi, K.; Imatsu, M.; Ide, K.; Shimada, J. Effects on fluvial discharges of the 2016 Kumamoto earthquakes, Japan. *J. Hydrol.* **2020**, *583*, 124600. [[CrossRef](#)]
71. Qiu, S.; Wang, F.; Dong, F.; Tian, F.; Zhao, X.; Dai, Q.; Li, Q.; Zhu, Y.; Wang, Y. Sedimentary evolution of the Dawan travertines and their geological environmental significance, Huanglong, China. *Depos. Rec.* **2022**, *8*, 251–265. [[CrossRef](#)]

Disclaimer/Publisher’s Note: The statements, opinions and data contained in all publications are solely those of the individual author(s) and contributor(s) and not of MDPI and/or the editor(s). MDPI and/or the editor(s) disclaim responsibility for any injury to people or property resulting from any ideas, methods, instructions or products referred to in the content.